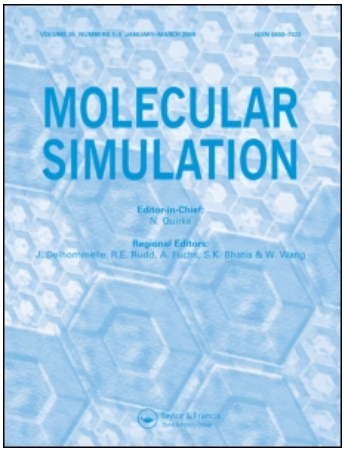

Molecular Simulation
Publication details, including instructions for authors and subscription information:
http://www.informaworld.com/smpp/title~content=t713644482

Isobaric and Isothermal Molecular Dynamics Simulations of Diatomic Systems

Vinayak N. Kabadi[a]; William A. Steele[b]
[a] Department of Chemical Engineering, North Carolina A&T State University, Greensboro, NC, U.S.A.
[b] Department of Chemistry, The Pennsylvania State University, University Park, PA, U.S.A.

To cite this Article Kabadi, Vinayak N. and Steele, William A.(1990) 'Isobaric and Isothermal Molecular Dynamics Simulations of Diatomic Systems', Molecular Simulation, 4: 6, 371 — 398
To link to this Article: DOI: 10.1080/08927029008022401
URL: http://dx.doi.org/10.1080/08927029008022401

Molecular Simulation, 1990, Vol. 4, pp. 371–398
Reprints available directly from the publisher
Photocopying permitted by license only

ISOBARIC AND ISOTHERMAL MOLECULAR DYNAMICS SIMULATIONS OF DIATOMIC SYSTEMS

VINAYAK N. KABADI

Department of Chemical Engineering, North Carolina A&T State University, Greensboro, NC 27411, U.S.A.

and

WILLIAM A. STEELE

Department of Chemistry, The Pennsylvania State University, University Park, PA 16802, U.S.A.

(*Received January 1989, accepted July 1989*)

Isobaric molecular dynamics simulations were carried out for diatomic systems using different algorithms available in the literature. Two-centered Lennard-Jones potentials with and without quadrupolar interactions were used. Thermodynamic properties obtained from the isobaric algorithms compared very well with those of an equivalent simulation in the microcanonical ensemble; however, some differences were observed when similar comparisons were carried out for dynamic properties. More specifically, the constant pressure constraint affects the translational dynamics of the system because of the non-negligible differences between the momenta and the instantaneous velocities of the molecules.

Furthermore, the following studies were carried out using isobaric MD simulations: 1. Low temperature spontaneous FCC-orthorhombic (and vice versa) transition of a diatomic system with quadrupolar interactions as a function of the molecular bond length. 2. Effect of quadrupolar interaction on isobaric melting of a model diatomic system. 3. Effect of pressure on melting properties of a model diatomic system with quadrupolar interactions.

KEY WORDS: Diatomic systems, isobaric simulations, melting, molecular dynamics, quadrupolar interactions.

1. INTRODUCTION

Molecular dynamics computer simulations are most easily performed in a microcanonical ensemble (N, V, E constant) and most MD simulation studies have been restricted to this ensemble. Whereas this technique is suitable for thermodynamic and dynamic studies of single phases, some phenomena such as phase transitions and phase coexistence are better studied at constant pressure. Of the constant pressure MD algorithms available in the literature, we study here the Andersen algorithm [1] and the Evans and Morriss algorithm [2]. The two methods are equivalent in all respects except in the method of applying the constant pressure constraint. Andersen's algorithm allows pressure to fluctuate, maintaining the average pressure constant, as opposed to the Evans-Morriss algorithm, which is designed to maintain the instantaneous pressure constant at the desired value at all times. Parrinello and Rahman

[3,4] extended Andersen's algorithm to allow for fluctuations in the shape as well as the size of the MD cell. In this technique the shape of the MD cell and hence the crystal lattice is changed to relieve the shear stress in the sample; thereby making it easier to predict solid—solid phase transitions. Another isothermal isobaric MD algorithm has been recently proposed by Berendsen *et al.* [5]. This is based on adjustable coupling of the system with an external bath held at the desired temperature and pressure.

Isobaric MD simulations were first applied to molecular systems by Pawley and Thomas [6] in their study of the transition from plastic to triclinic crystalline phase of SF_6 at zero pressure. They maintained pressure constant to a desired value by systematic scaling of molecular positions. Their algorithm, however, was essentially a (N, V, E) algorithm. Later, Nosé and Klein [7] extended the Andersen-Parrinello-Rahman (APR) algorithm to molecular systems and studied high pressure solid—solid phase transitions of nitrogen [8] and low pressure solid—plastic—liquid phase transition of CF_4 [9]. Ryckaert and coworkers [10,11] have further extended the APR algorithm to non-rigid polyatomic molecules, and more recently, Coon and coworkers [12] have used the APR algorithm to study mixtures of diatomic liquids.

MD simulations in the microcanonical ensemble result in fluctuations and hence uncertainties in the system temperature, calculated as a time average of the system kinetic energy (or "kinetic temperature"). This is undesirable especially when thermodynamic and dynamic properties are to be determined at a precise temperature, e.g. in the determination of solid—solid and solid—liquid transition temperatures. Algorithms for isothermal MD simulations are therefore required. A few different such algorithms are available; the first one is due to Andersen [1] and maintains constant temperature by changing the kinetic energies of the atoms by applying stochastic forces. This is, however, not a very useful algorithm if dynamic properties are to be studied because it results in unsmooth molecular trajectories. The second algorithm, due to Evans and coworkers [2, 13, 14] involves the modification of the force acting on a molecule by addition of a force of constraint linear in the momentum of the molecule and of magnitude adjusted to maintain constant system kinetic energy. This method maintains the kinetic temperature identically constant but results in non-canonical equations of motion. On the other hand, Nosé [15, 16] has devised an algorithm which generates canonical rather than isothermal equilibrium distributions. In the thermodynamic limit, both the Evans and the Nosé algorithms yield the correct time correlation functions [17]. Another algorithm due to Haile and Gupta [18] involves continuous scaling of momenta and has the same disadvantage as Andersen's algorithm. Jellinek [19] has recently devised a generalized unified scheme for dynamical simulation of any statistical ensemble, and has analyzed the algorithms for the canonical ensemble as an example.

In this work, we have used the Evans-Morriss (EM) algorithm with cubic MD cell and Andersen-Parrinello-Rahman (APR) algorithm with variable MD cell shape, to carry out constant pressure simulations of molecular fluids interacting by multiple-centered LJ site—site potential with and without quadrupolar interactions. For isothermal MD simulations we have used the method of Evans and coworkers. In the first part of the paper, we briefly review the algorithms. Next, we compare the thermodynamics and dynamics of model diatomic systems in solid and liquid phases obtained from simulations using three different algorithms, namely, the microcanonical MD, the APR or Nosé-Klein algorithm and the extended Evans-Morriss isothermal-isobaric algorithm. This is followed by a description of studies carried out using

isobaric MD: 1. FCC to orthorhombic (and vice versa) transition at low temperature of a model site-site diatomic with quadrupolar interactions as a function of the molecular bond length and 2. Effect of quadrupole moment and pressure on isobaric melting of a model diatomic system.

2. ISOBARIC AND ISOTHERMAL MD ALGORITHMS

Cubic MD Cells

Andersen and EM algorithms for isobaric MD simulations of atomic systems are equivalent as far as the expressions for molecular motions are concerned, but because of the different methods used to impose the constant-pressure constraint, the constraint equations and parameters take different forms.

Consider a cubic MD cell of volume V and each side $V^{1/3}$ (V is a function of time). Let $\tilde{q}_i$ denote the coordinates of the positions of atoms and $\tilde{p}_i$ the components of their momenta. Andersen formulated his equations of motion in an MD cell of unit length. Denoting the atomic positions in such a cell by $\tilde{s}_i$ we may write.

$$\tilde{q}_i = V^{1/3}\,\tilde{s}_i \tag{1}$$

The Lagrangian of the system of N atoms each of mass m may be written as

$$\mathscr{L} = \sum_{i=1}^{N} \tfrac{1}{2}\, m\, V^{2/3}\, \tilde{\dot{s}}_i \cdot \tilde{\dot{s}}_i - u(\tilde{q}_{ij}) \tag{2}$$

For the coordinates $\tilde{s}_i$ the conjugate momenta $\tilde{p}_{si}$ are given as

$$\tilde{p}_{si} = m\, V^{2/3}\, \dot{s}_i \tag{3}$$

The Hamiltonian for the conjugate pair $(\tilde{s}_i, \tilde{p}_{Si})$ is

$$H(\tilde{s}_i, \tilde{p}_{si}) = \sum_{i=1}^{N} \tfrac{1}{2}\, m\, V^{2/3}\, \tilde{\dot{s}}_i \cdot \tilde{\dot{s}}_i + \sum_{i<j=1}^{N} u\,(\tilde{q}_{ij}) \tag{4}$$

from which the equations of motion may be written as

$$\tilde{\dot{p}}_{si} = V^{1/3}\, \tilde{F}_i \tag{5}$$

$$\tilde{\ddot{s}}_i = \frac{1}{m\, V^{1/3}}\, \tilde{F}_i - \frac{2}{3}\, \tilde{\dot{s}}_i \frac{\mathrm{d} \ln V}{\mathrm{d}\, t} \tag{6}$$

where $\tilde{F}_i$ is the force acting on atom i. These are Andersen's equations of motion. In terms of coordinates $\tilde{q}_i$ and conjugate momenta $\tilde{p}_i$, the Hamiltonian may be written as

$$H(\tilde{q}_i, \tilde{p}_i) = \sum_{i=1}^{N} \frac{\tilde{p}_i \cdot \tilde{p}_i}{2\, m} + \sum_{i=1}^{N} \frac{\dot{V}}{3V}\, \tilde{q}_i \cdot \tilde{p}_i + \sum_{i<j=1}^{N} u\,(\tilde{q}_{ij}) \tag{7}$$

The equations of motion then become

$$\tilde{\dot{q}}_i = \tilde{p}_i + \dot{\varepsilon}\, \tilde{q}_i \tag{8}$$

$$\tilde{\dot{p}}_i = \tilde{F}_i - \dot{\varepsilon}\, \tilde{p}_i \tag{9}$$

where

$$\dot{\varepsilon} = \frac{\dot{V}}{3\, V} \tag{10}$$

$\dot{\varepsilon}$ is called the dilation rate of the MD cell. Equations (8) and (9) represent the equations of motion as given by Evans and Morriss. Equation (6) and Equations (8) and (9) are thus equivalent. To be able to use these equations, however, the time dependence of the cell volume or the dilation rate $\dot{\varepsilon}$ should be known. Andersen and Evans-Morriss employed quite different techniques to maintain constant pressure. Andersen assumed that the MD cell is exposed to an external bath which is kept at the desired constant pressure P_{ext}. The cell is separated from the bath by a thin flexible membrane. The volume of the MD cell fluctuates in response to the difference between the internal and the external pressure. The dilation of the volume is governed by the conjugate coordinate-momentum pair (V, p_v) with

$$p_v = M\dot{V} \tag{11}$$

where M is the measure of the mass of the membrane (it has units of mass × -length^{-4}). From the total Hamiltonian including terms due to volume changes, the dynamic equation for the volume dilation may be shown to be[1]

$$M\, \mathrm{d}^2V/\mathrm{d}t^2 = (P - P_{ext}) \tag{12}$$

where P is the instantaneous system pressure given as

$$P = 1/3V\left[\sum_{i=1}^{N} \tilde{p}_i \cdot \tilde{p}_i/m + \sum_{i<j=1}^{N} \tilde{q}_{ij} \cdot \tilde{F}_{ij}\right] \tag{13}$$

This method makes it possible to control the average simulation pressure to the desired value but pressure fluctuates during the simulation, the fluctuations depending on the fictitious mass M of the membrane.

In contrast, Evans and Morriss calculate the dilation rate $\dot{\varepsilon}$ at every time step by directly imposing the presssure constraint. Taking the time derivative of equation (13) setting $\dot{P} = 0$ and using equation (10) we get

$$9PV\dot{\varepsilon} = \sum_{i=1}^{N} 2\,\tilde{p}_i \cdot \dot{\tilde{p}}_i/m + \sum_{i<j=1}^{N} (\dot{\tilde{q}}_{ij} \cdot \tilde{F}_{ij} + \tilde{q}_{ij} \cdot \dot{\tilde{F}}_{ij}) \tag{14}$$

from which $\dot{\varepsilon}$ may be calculated. This method, which is based on Gauss' principle of least constraint, is designed to maintain the system pressure identically constant. However, one must use artificial gradients to bring the pressure to the desired value to start the simulation, and also, if the pressure wanders slightly during the simulation there is no systematic way to bring it back to the desired value. If the volume dilation is such that the pressure is identically constant, it may be easily shown that for the Hamiltonian given by Equation (4) or Equation (7) the time evolution of the system has to follow an isobaric-isoenthalpic path [1, 2, 18].

Recently, Edberg *et al.* [21] have developed a simulation method for long chain flexible molecules that uses the Gauss' principle of least constraint to constrain the bond lengths and bond angles to desired values.

Of the various isothermal MD algorithms available [1, 2, 13–19] we discuss only the algorithm of Evans and Morriss [2] as it is the only algorithm that is designed to maintain the temperature identically constant while giving smooth molecular trajectories. It involves adding a force of constraint linear in momentum to the rate of change of linear momentum e.g. for isobaric-isothermal simulation, Equation (9) is modified as

$$\dot{\tilde{p}}_i = \tilde{F}_i - \dot{\varepsilon}\,\tilde{p}_i - \alpha\,\tilde{p}_i \tag{15}$$

α is evaluated by direct application of constant temperature constraint, which is

$$\sum_{i=1}^{N} \tilde{p}_i \cdot \dot{\tilde{p}}_i = 0 \tag{16}$$

Substituting Equation (15) in Equation (16) and using equation (14), $\dot{\varepsilon}$ and α may be evaluated at each time step thereby maintaining pressure and temperature constant.

Extensions of the above algorithms to molecular systems is straightforward. The Hamiltonian is modified by the addition of extra terms because of the rotational motion of the molecules. Specifically,

$$H_{\text{rot}} = 1/2 \sum_{i=1}^{N} \tilde{\omega}_i \cdot \mathbf{I}_i \cdot \tilde{\omega}_i \tag{17}$$

where $\tilde{\omega}_i$ and $\mathbf{I}_i$ are angular velocity vector and moment of inertia tensor respectively of the molecule i. The number of terms in the rotational Hamiltonian may be reduced by transforming the angular velocities to the principal axis frame. The rotational equations of motion for each molecule are then the usual Euler Equations [22].

$$\mathbf{I} \cdot \dot{\tilde{\omega}} + \tilde{\omega} \times (\mathbf{I} \cdot \tilde{\omega}) = \tilde{N} \tag{18}$$

where the components of the moment of inertia $\mathbf{I}$, angular velocity $\tilde{\omega}$, and torque $\tilde{N}$ are written in the principal axis frame.

For isobaric-isoenthalpic MD simulation equation (18) is solved simultaneously with either Equation (6) or Equation (8) and (9). The forces and torques acting on individual molecules are calculated in the usual manner [23]. It should be noted that the constant pressure constraint does not affect the rotational motion of the molecules directly. For isobaric-isothermal MD Equation (18) is modified by adding $-\alpha_1(\mathbf{I} \cdot \tilde{\omega})$ to the right hand side. The new equation so obtained will be denoted by Equation (18a). α_1 is then evaluated by applying the constant temperature constraint to the rotational degrees of freedom. Thus,

$$\sum_{i=1}^{N} (I_{px}\omega_{px}\dot{\omega}_{px} + I_{py}\omega_{py}\dot{\omega}_{py} + I_{pz}\omega_{pz}\dot{\omega}_{pz}) = 0 \tag{19}$$

Substituting for $\dot{\omega}_{px}, \dot{\omega}_{py}, \dot{\omega}_{pz}$ from Equation (18a) one obtains and equation for α_1, which is calculated together with α at each time step, so that both translational and rotational kinetic energies satisfy the constant temperature constraint. The detailed Equations for the pressure and the temperature constraint of the Evans-Morriss isothermal-isobaric algorithm as applied to homonuclear diatomic systems with ideal point quadrupoles are given in the appendix.

Variable MD Cell Shape

Parrinello and Rahman [3,4] modified Andersen's algorithm to allow for variations in the shape as well as the size of the MD cell. This technique makes it possible to obtain solid—solid phase transitions in a MD simulation. The MD cell shape is changed to relieve the shear stress in the sample. In a real system this should happen naturally by molecular motions; however, in a MD simulation with limited number of molecules, shear stress relaxation and hence spontaneous changes in lattice structures are not easily attainable.

In what follows, we briefly discuss the Parrinello-Rahman algorithm and an equiva-

lent extention of the Evans-Morriss algorithm as applied to molecular systems. The MD cell is described by a 3 × 3 matrix **h** the columns of which represent the three vectors $\tilde{a}_1$, $\tilde{a}_2$, $\tilde{a}_3$ that define the edges of the MD cell. The transformation from the coordinates of the center of mass of a molecule i in the real MD cell to a cubic cell of unit length is given by

$$\tilde{q}_1 = \mathbf{h}\tilde{s}_1 \tag{20}$$

For the coordinates $\tilde{s}_1$ the conjugate momenta $\tilde{p}_{si}$ are

$$\tilde{p}_{si} = m\,\mathbf{G}\,\dot{\tilde{s}}_i \tag{21}$$

The Hamiltonian for the conjugate coordinate-momentum pair $(\tilde{s}_i, \tilde{p}_{si})$ is then given by

$$H(\tilde{s}_i, \tilde{p}_{si}) = \tfrac{1}{2} m \sum_{i=1}^{N} \dot{\tilde{s}}_i^t\,\mathbf{G}\,\tilde{s}_i + \sum_{i<j=1}^{N} u\,(\tilde{q}_{ij}) \tag{22}$$

where

$$\mathbf{G} = \mathbf{h}^t\mathbf{h} \tag{23}$$

The translational Equations of motion may now be written as

$$\dot{\tilde{s}}_i = 1/m\,\mathbf{h}^{-1}\,\tilde{F}_i - \mathbf{G}^{-1}\dot{\mathbf{G}}\,\dot{\tilde{s}}_i \tag{24}$$

To derive the Equations of motion equivalent to the Evans-Morriss algorithm (Equations (8) and (9), we work with conjugate coordinate-momentum pair $(\tilde{q}_i, \tilde{p}_i)$. The Hamiltonian is given by

$$H = 1/2m \sum_{i=1}^{N} \tilde{p}_i \cdot \tilde{p}_i + \sum_{i=1}^{N} \tilde{q}_i^t\,\dot{\varepsilon}\,\tilde{\mathbf{P}}_i + \sum_{i<j=1}^{N} u(\tilde{q}_{ij}) \tag{25}$$

where $\dot{\boldsymbol{\varepsilon}}$ is the dilation rate tensor defined by

$$\dot{\mathbf{h}} = \dot{\boldsymbol{\varepsilon}}^t\mathbf{h} \tag{26}$$

The translational Equations of motion are now

$$\dot{\tilde{q}}_i = \tilde{p}_i/m + \dot{\boldsymbol{\varepsilon}}^t\tilde{q}_i \tag{27}$$

$$\dot{\tilde{p}}_i = \tilde{F}_i - \dot{\boldsymbol{\varepsilon}}\tilde{p}_i \tag{28}$$

Equation (24) and Equations (27) and (28) are again equivalent. However, as before different methods are employed to evaluate the time dependence of matrix **h**.

In the APR algorithm it is assumed that the MD cell is surrounded by a flexible membrane of mass M which separates the cell from an infinite bath kept at the constant desired pressure $\mathbf{P}_{ext}$. The fluctuations in the shape and size of the MD cell are then governed by the following equation

$$M\ddot{\mathbf{h}} = (\boldsymbol{\pi} - P_{ext})\,\boldsymbol{\sigma} \tag{29}$$

where $\boldsymbol{\pi}$ is the pressure or shear stress tensor for the sample

$$\boldsymbol{\pi}V = \sum_{i=1}^{N} \tilde{p}_i\,\tilde{p}_i/m + \sum_{i<j=1}^{N} \tilde{F}_{ij}\tilde{q}_{ij} \tag{30}$$

V is the volume of the MD cell

$$V = \tilde{a}_1 \cdot (\tilde{a}_2 \times \tilde{a}_3) \tag{31}$$

and $\boldsymbol{\sigma}$ is a tensor of cross sections given as

$$\boldsymbol{\sigma} = \{\tilde{a}_2 \times \tilde{a}_3, \tilde{a}_3 \times \tilde{a}_1, \tilde{a}_1 \times \tilde{a}_2\} \tag{32}$$

The Evans-Morriss method of applying the pressure constraint may also be extended to this case. Taking the time derivative of Equation (30) and setting $\dot{\pi} = 0$ we obtain.

$$\pi \dot{V} = \sum_{i=1}^{N} (\dot{\tilde{p}}_i \tilde{p}_i + \tilde{p}_i \dot{\tilde{p}}_i)/m + \sum_{i<j=1}^{N} \dot{F}_{ij} \tilde{q}_{ij} + \tilde{F}_{ij} \dot{\tilde{q}}_{ij} \tag{33}$$

$\dot{V}$ is obtained by taking the derivative of Equation (31) and may be written in terms of components of $\dot{\boldsymbol{\varepsilon}}$

$$\dot{V} = \sum_{i=1}^{3} \sum_{j=1}^{3} \left[\sum_{k=1}^{3} (\tilde{a}_m \times \tilde{a}_n)_j (\tilde{a}_k)_i \right] \dot{\varepsilon}_{ij} \tag{34}$$

where $m, n = 1,2; 2,3; 3,1$, and $m \neq n \neq k$.

Substituting proper expressions for $\dot{\tilde{p}}_i$, $\dot{F}_{ij}$ and $\dot{\tilde{q}}_{ij}$ in equation (33), we get nine equations for nine components of $\dot{\boldsymbol{\varepsilon}}$ which are then easily calculated. The rotational equations of motion and the isothermal constraint equations may be formulated in this case exactly the same way as in the case of cubic MD cell, because these are not directly affected by the constant pressure constraint.

One of the problems in using the above algorithms based on variable MD cell shape is that the MD cell as a whole undergoes rotation because of non-conservation of the angular momentum in the MD cell. The rotations may also be interpreted as caused by the instantaneous asymmetry of the shear stress tensor. This does not affect the equilibrium thermodynamics of the system but may cause serious difficulties in calculating the translational time correlation functions. Nosé and Klein [7] have dealt with this problem in detail and have suggested an approximate method to prevent the cell rotation.

Two specific algorithms have been used in the MD simulations reported in this work: 1. The APR algorithm for molecular systems, which is represented by Equations (18), (24) and (29). No attempt has been made to prevent the MD cell rotation. This will be denoted as APR–NK algorithm (NK stands for Nosé and Klein who were the first to report simulations using this algorithm). 2. The isothermal-isobaric Evans and Morriss algorithm as applied to molecular systems, in cubic MD cell or more specifically Equations (8), (10), (14), (15), (16), (18a) and (19). This will be referred to as the extended Evans-Morriss algorithm or simply the EEM algorithm.

3. SIMULATIONS AND COMPARISON BETWEEN DIFFERENT ALGORITHMS

In this part of the work, we compare the three MD algorithms, namely, NVE, APR–NK and EEM. All three methods are expected to give comparable equilibrium thermodynamic properties, and configurational distribution functions [15,16,24,25]. It has also been shown that the EEM algorithm gives time correlation functions which differ from the equivalent functions obtained from Newtonian dynamics by terms of 0(1/N) which dissapear in the thermodynamic limit. Yet, the differences in the

fluctuations of the variables and in the individual molecular dynamics when the three algorithms are used in MD simulations with limited number of molecules are not obvious and have not been properly investigated. This is the purpose of the following study. Brown and Clarke [26] did precisely such a study for atomic systems using Andersen's isobaric algorithm, different available isothermal algorithms and the classical NVE MD algorithm. They, however, did not find any appreciable differences between the results obtained with any of these algorithms.

Potential and Simulation Method

Simulations were carried out with 256 homonuclear diatomic molecules arranged in a MD cell with periodic boundary conditions. The potential energy of a pair of molecules was taken to be the sum of site-site LJ interactions plus point quadrupole-quadrupole interaction. Thus,

$$u(q_{ij},\theta_i, \theta_j, \phi_{ij}) = u^{DI}(q_{ij}, \theta_i, \theta_j, \phi_{ij}) + u^{QQ}(q_{ij}, \theta_i, \theta_j,\phi_{ij}) \quad (35)$$

$$u^{DI} = \sum_{k=1}^{2}\sum_{l=1}^{2} 4\varepsilon\,[(\sigma/r_{kl})^{12} - (\sigma/r_{kl})^{6}] \quad (36)$$

$$u^{QQ} = 3\,Q^2/q_{ij}^5\,[1 - 5(\cos^2\theta_i + \cos^2\theta_j) + 2(\sin\theta_i \sin\theta_j \cos\phi_{ij} - 4\cos\theta_i \cos\theta_j)^2 - 15\cos^2\theta_i\cos^2\theta_j] \quad (37)$$

where r_{kl} is the separation distance between site k on molecule i and site l on molecule j. θ_i, θ_j, and ϕ_{ij} are the polar and the azimuthal angles which describe the relative orientations of two axially symmetric linear molecules.

For comparison of the APR–NK and the EEM algorithms with the NVE MD method, two model potentials and two state conditions, (a liquid and a solid), were chosen; (1) Liquid - L* (bond length/σ) = 0.547, $Q^* = 0$, $T^* = 1.50$, $P^* = 0.15$, $\rho^* = 0.522$; (2) Solid - $L^* = 0.547$, $Q^* = 1.0$, $T^* = 1.34$, $P^* = 0.20$, $\rho^* = 0.628$. Simulations were carried out for these two state points using each of the three MD algorithms. Runs were normally started from a face-centered-cubic α-N_2 structure. Time steps in the range of 0.0003 to 0.0010 reduced units were used. A cutoff distance of 3σ to 3.5σ was used for the calculation of forces and torques. Corrections were made for the contributions to pressure and energy due to long-ranged interactions, assuming that there is no correlation between pairs of molecules separated by distances greater than the cut-off distance. For the APR–NK and EEM MD the long-range corrections have to be evaluated at each time step of the simulation because of the fluctuating system density.

For the EEM algorithm, the pressure was initially brought to the desired value P_{ext} by adding a term proportional to the difference between the instantaneous system pressure and the desired pressure arbitrarily to the left hand side of Equation (16). This external pressure gradient was maintained through most of the equilibration stage and then slowly removed as the pressure held constant at the desired value. This procedure worked very well for the simulations with $Q^* = 0$. However, when the quadrupolar potential was introduced, the pressure fluctuated around the desired value with maximum fluctuations of $\pm$ 0.15 reduced units. We attribute these fluctuations to the long range nature of the quadrupolar potential; to maintain pressure identically constant for these systems, the size of the MD cell and hence the number of molecules should be increased, thereby increasing the maximum possible cut-off

distance. (Further studies in that direction are under way. Attempts are also being made to apply this constant pressure algorithm to systems with discrete charge distributions.) For the purposes of the present study, however, these small fluctuations in pressure are not expected to affect the results appreciably.

Comparisons of thermodynamic and dynamic properties obtained from the three algorithms for the two state points are presented in the following sections. Reduced units are used in the presentation of results the reducing parameters being the molecular mass m, and the potential parameters σ and ε.

Equilibrium Thermodynamics and Structure

Equilibrium thermodynamic properties in the form of temperature, pressure, density and configurational internal energy for the two state points are given in Table 1. Simulations for the liquid were carried out solely for the purposes of the comparison of the NVE, APR-NK and the EEM algorithms. This is reflected by the identical conditions of temperature, pressure and density for the three simulations. The solid simulations, however, were a part of other studies (see Section 5 and Kabadi and Steele [27]). The conditions here are therefore not identical but close enough to allow for direct comparisons. In general all three algorithms show excellent agreement in the values of the equilibrium thermodynamic properties. Differences in the configurational internal energies observed for the solid can be accounted for by the differences in the temperatures and the densities.

The configurational internal energies and the pressures or densities (pressure for NVE and densities for APR-NK and EEM) in Table 1 are calculated as averages of proper quantities during the simulations. Although these average quantities are equivalent for the three algorithms, the instantaneous values of these quantities and their fluctuations are quite different. In the NVE simulation, the pressure, the kinetic energy and the potential energy fluctuated around the mean, with a maximum fluctuation in pressure of about 1.8 reduced units. In the EEM simulation, the temperature was identically constant. The pressure was constant for the $Q^* = 0$ run but fluctuated by ± 0.15 reduced units every 100 time steps for $Q^* = 1$; as was expected the potential energy and the enthalpy also fluctuated. In contrast, in the APR-NK simulation none of these quantities were strictly constants of motion; both the pressure and the volume fluctuated with a maximum pressure fluctuation of almost 1 reduced unit.

The fluctuations of proper quantities in different ensembles allow one to calculate

Table 1 Equilibrium Thermodynamic Properties with NVE, APR-NK and EEM Algorithms.

	N_t	$t^* \times 10^4$	T^*	P^*	ρ^*	E^*
(Liquid; $L^* = 0.547$, $Q^* = 0$)						
NVE	5000	5	1.499	0.18	0.522	−13.26
APR-NK (M = 0.20)	5000	5	1.499	0.09	0.522	−13.27
EEM	5000	5	1.500	0.10	0.522	−13.29
(Solid; $L^* = 0.547$, $Q^* = 1.0$)						
NVE	10000	2	1.386	0.31	0.625	−18.53
APR-NK ($M = 2.0$)	5000	5	1.306	0.09	0.633	−19.00
EEM	5000	5	1.340	0.17	0.629	−18.78

*Note: N_t is the number of time steps after equilibration and t^* is the length of each time step in reduced units.

thermodynamic properties, e.g. fluctuations of potential energies and the pressure virial are related to the constant volume heat capacity C_v and the adiabatic compressibility (β_s) in the microcanonical ensemble and to C_v and the isothemal compressibility (β_t) in the canonical ensemble [28,29]. Similarly fluctuations in $\Phi + P/\rho$ (Φ is the instantaneous potential energy per molecule) and volume provide a means for calculation of constant pressure heat capacity C_p and β_s in the isobaric-isoenthalpic ensemble and of C_p and β_T in the isobaric-isothermal ensemble [30,31]. In particular, C_p may be calculated in the two ensembles from the following equations

$$C_p/k = \nu/2[1 - N\beta^2/(\nu/2)\langle(\delta H)^2 | NPH]\rangle^{-1} \tag{38}$$

$$C_p/k = \nu/2 + N\beta^2\langle(\delta H)^2 | NP\beta\rangle \tag{39}$$

where $H = (\Phi + P/\rho)$ and ν represents the total number of degrees of freedom for the molecular motion.

Calculation of thermodynamic properties from fluctuations generally requires very high numerical precision because it involves subtraction of two large numbers. We attempted the computation of C_p from Equation (38) for APR–NK and from Equation (39) for EEM MD simulations. We were not able to obtain values for C_p with high confidence limits. However, we did find that Equation (38) with APR–NK MD gave negative values for C_p of the solid. (This was also found to be true for the other solid simulations reported later in the paper, Table 3). We attribute this to the fact that neither the pressure nor the enthalpy were conserved in our APR–NK simulations. With this algorithm, the quantity that is conserved is the enthalpy of the system plus the kinetic energy of the hypothetical membrane, and the simulation approaches isobaric-isoenthalpic simulation when the fluctuations in the membrane kinetic energy are negligible. In our simulations, the kinetic energy of the membrane fluctuated appreciably thereby causing large fluctuations in both the pressure and the enthalpy of the system. As a result, Equation (38) is not appropriate to calculate C_p in these cases. For the EEM MD Equation (39) gave reasonable values of C_p for the $Q^* = 0$ run, but for $Q^* = 1$ run very large fluctuations in C_p made it impossible to obtain an average value. Hence, for accurate calculations of C_p and other properties from the fluctuation formulae, the fluctuations in pressure obtained in the EEM algorithm should be reduced, probably by taking a larger cut-off distance (or by using cut-off potentials).

We also compared the structure of the systems simulated using the three algorithms. For the points listed in Table 1 we computed the spherical harmonic coefficients [32,33] of the molecular pair correlation function (pcf). The pcf is defined so that $\rho_N^{(1)} g(r, \omega_1, \omega_2) dV$ gives the number of molecules at a distance r, in orientation ω_2 and in a volume element dV around the central molecule defined by orientation ω_1. In microcanonical and cononical ensembles $\rho_N^{(1)}$ is simply the system density. $\rho_N^{(1)}$ in NPH and NPT ensembles is given by $N/\langle V\rangle$ where $\langle V\rangle$ is the expectation value of the volume. The expression for $\rho_N^{(1)}$ for the APR–NK algorithm is not clear, but we computed the spherical harmonic coefficients ($g_{11,m}$) of the pcf assuming that this algorithm represents a NPH ensemble. In Figures 1 and 2 we have plotted g_{000}, g_{200} and g_{220} of the liquid and the solid as computed using each of the three algorithms. The results from the three methods are almost identical as indicated by the curves sitting on top of one another. This is true even for the solid where the simulation conditions for the three methods were not identical.

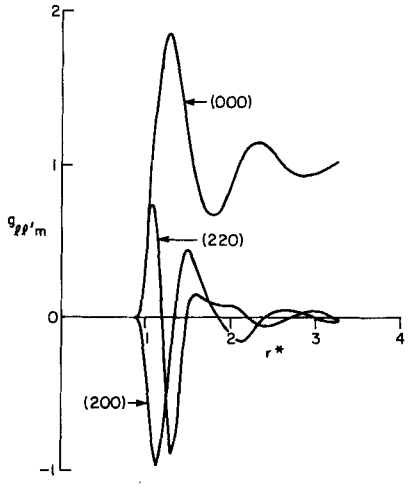

Figure 1 Coefficients of the spherical harmonic expanstion of the simulated pair correlation functions for the three liquid state points of Table 1. The three curves correspsonding to the NVE, APR–NK and EEM algorithms for each of the coefficients overlap and are indistinguishable.

Dynamics of Individual Molecules

Evans and Morriss [34] have shown that the time correlation functions obtained from the Gaussian isothermal dynamics should be identical to the ones obtained from the Newtonian dynamics in the thermodynamic limit. In addition, Brown and Clarke [26] did MD simulations with 256 LJ atoms and concluded that the individual molecular dynamics obtained from the Andersen's isobaric algorithm and different available isothermal algorithms were indistinguishable from the equivalent properties cal-

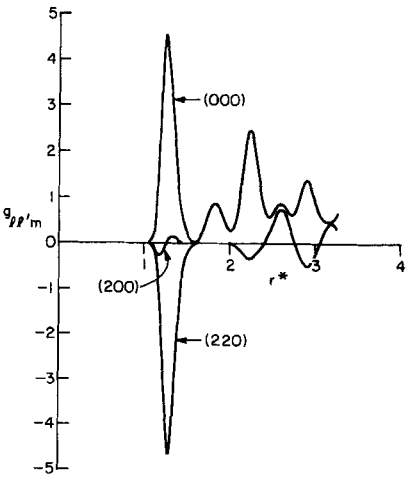

Figure 2 Same as Figure 1 but for the solid state points of Table 1.

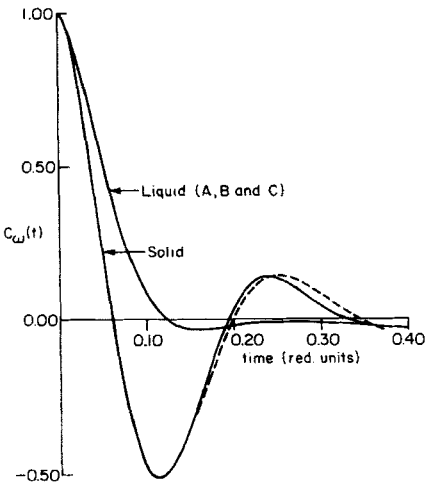

Figure 3 Angular velocity time correlation functions are shown for the liquid and the solid state points of Table 1. The three curves are indicated by (A) NVE. (B) APR-NK and (C) EEM. The curves for the liquid state coincide with one another.

culated from the NVE MD. We have carried out such a study for the molecular systems using the APR-NK and the EEM algorithms.

The rotational dynamics of the molecules is not affected at all by the constant pressure constraint. Even the isothermal constraint in the EEM algorithm seems to have little effect on these time correlations. This is indicted by Figures 3–5, where we have plotted the normalized angular velocity time correlation functions $C_\omega(t^*)$ and the first three reorientational correlation functions $C_l(t^*)$ defined in the usual way

$$C_l(t^*) = \langle P_l \cos\delta\theta(t^*) \rangle \tag{40}$$

where P_l is the Legendre function and $\delta\theta$ is the reorientation angle of the molecular axis. For the liquid, the slight differences observed in $C_l(t^*)$ obtained from the three MD methods (Figure 4) are within the limits of statistical errors. Larger differences observed between the curves of $C_\omega(t^*)$ and $C_l(t^*)$ for the solid may be explained by the differences in the temperatures and the densities of the three simulations. For instance the NVE MD simulation is at the highest temperature ($T^* = 1.386$) and the lowest density ($\rho^* = 0.625$) and the fact that $C_l(t^*)$ decays most rapidly for this method merely indicates slightly smaller torques for this state point.

The comparison of the translational dynamics is not that straightforward. The isobaric constraint results in the velocity of a molecule ($\dot{q}$) being different than the one calculated from its momentum ($\tilde{p}/m$) (the relations are given by Equation (8) for the cubic MD cell and Equation (27) for the variable shape MD cell). One can thus obtain two different velocity time correlations

$$C_v(t) = \langle \tilde{\dot{q}}(t) \cdot \tilde{\dot{q}}(0) \rangle \tag{41}$$

$$C_m(t) = 1/m \langle \tilde{p}(t) \cdot \tilde{p}(0) \rangle \tag{42}$$

In general, these would be different for a system of finite size, and would be equal to each other and equal to the velocity time correlation obtained from Newtonian

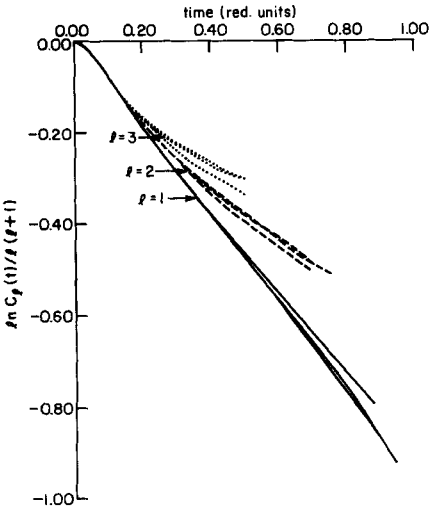

Figure 4 Orientational time correlation functions $C_l(t)$ for $l = 1,2$ and 3 are shown for the liquid state points of Table 1.

dynamics only in the thermodynamic limit. We computed $C_v(t)$ and $C_m(t)$ ($C_v = C_m$ for the NVE simulation) for the liquid and solid simulations of Table 1. These are plotted in Figures 6 and 7. In the APR–NK algorithm we did not attempt to stop the rotation of the MD cell; as a result the $C_v(t^*)$ for this case clearly show this effect and are very different from the rest of the functions. $C_m(t^*)$ for the APR–NK and the EEM simulations agree very well with the velocity correlations given by the NVE MD. On the other hand, $C_v(t^*)$ from the EEM simulations show slight deviations from the other three functions.

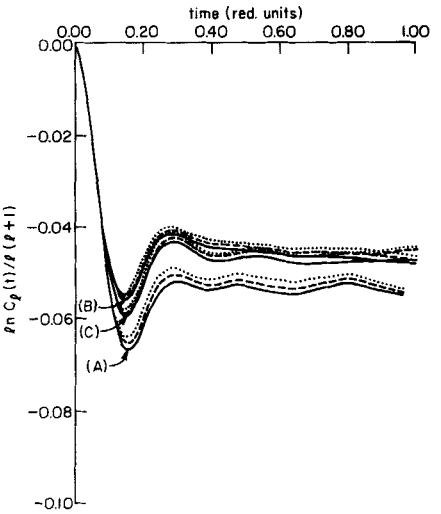

Figure 5 Same as Figure 4 but for the solid state points of Table 1.

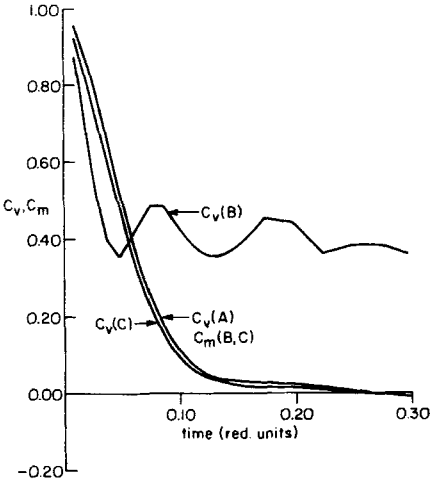

Figure 6 Translational velocity correlation functions are shown for the liquid state points of Table 1. A, B, and C denote the three MD methods as in Figure 3.

It therefore seems that one can obtain Newtonian dynamics in an isobaric MD by defining $C_m(t^*)$ as the velocity time correlation function. This, however, causes another problem in the definition of the self diffusion constant, D, for these systems. The self diffusion constant can be obtained from [35]

$$D = \tfrac{1}{3}\int_0^\infty \langle \tilde{q}(t) \cdot \tilde{q}(0) \rangle \, dt$$
$$= \tfrac{1}{3}\int_0^\infty c_v(t) \, dt \qquad (43)$$

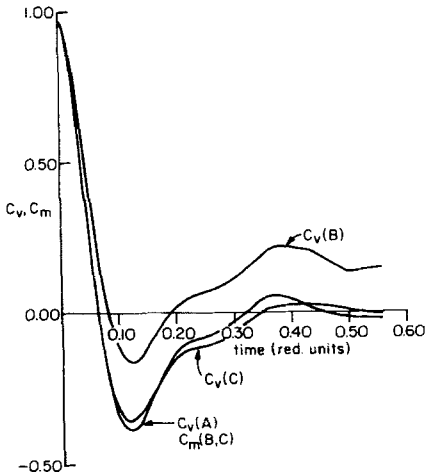

Figure 7 Same as Figure 6 but for the solid state points of Table 1.

For isobaric systems, substituting Equation (8) for $\dot{q}$ and putting cross correlations between $\tilde{q}$ and $\tilde{p}$ to zero we get

$$D = \tfrac{1}{3}\int_0^\infty \left[\frac{1}{m}\langle \tilde{p}(t)\cdot\tilde{p}(0)\rangle + \langle \dot{\varepsilon}(t)\,\tilde{q}(t)\cdot\dot{\varepsilon}(0)\,\tilde{q}(0)\rangle\right]dt$$

$$= \tfrac{1}{3}\int_0^\infty [c_m(t) + \langle \dot{\varepsilon}(t)\,\tilde{q}(t)\cdot\dot{\varepsilon}(0)\,\tilde{q}(0)\rangle]dt \qquad (44)$$

From Equation (44) we can see that D cannot be simply calculated from $C_m(t)$. Thus, although $C_m(t)$ provide velocity time correlation functions in isobaric MD that agree well with the corresponding functions in Newtonian dynamics, one should use $C_v(t)$ to calculate the self diffusion constant. For the liquid of Table 1 and other liquids (reported later in Table 3) simulated using the EEM algorithm, the average error in the self diffusion constant calculated from equation (43) and the corresponding value estimated for Newtonian dynamics was found to be 5%. This can be easily seen from Figure 8 where we have plotted the mean square displacements $\langle |\tilde{q}(t) - \tilde{q}(0)|^2 \rangle$. The long-time slopes of these curves should be proportional to the self diffusion constants. Difference in the slopes of the lines representing liquid (A) and liquid (C), therefore, is an estimate of the error in D calculated from the EEM simulation as compared to that in the Newtonian dynamics. Needless to say, Figure 8 again illustrates the need to stop the rotation of the MD cell in the APR–NK simulation if it is to be used for the study of translational dynamics of individual molecules.

In summary, we conclude that although the NVE, APR–NK and EEM algorithms give equivalent average thermodynamic and structural properties, they exhibit marked differences with respect to the calculations of thermodynamic properties from fluctuations and with respect to translational dynamics of individual molecules.

4. CUBIC Pa3 TO ORTHORHOMBIC CmCa TRANSITION OF DIATOMIC SOLIDS

English and Venables [36] made a detailed study of the lattice structures at low temperatures of real solids as well as solids made up of model molecules interacting by site-site LJ potentials with and without quadrupolar interactions. For the model solids they optimized the lattice parameters to give the minimum potential energy for a number of lattice structures and determined the most stable structure as the one with the minimum optimized potential energy. This way they were able to construct a chart for model diatomic systems giving regions of stability of different lattice structures with L^* (bond length to sigma ratio) and Q^* (reduced quadrupole moment) as parameters. Despite its great simplicity, this approach gave the correct structures for some real diatomic solids. One of the features observed in their study was that for quadrupole moments in excess of about 4×10^{-26} e.s.u. cm^2 there exists a L^* below which cubic Pa3 is the stable lattice structure and above which the stable lattice structure is orthorhombic CmCa. This tranistion L^* was found to increase slightly as the quadrupole moment was increased. Thus, at a constant temperature and pressure, as the bond length of the molecules is increased one should encounter a transition in solid structure from cubic Pa3 to orthorhombic CmCa.

Parrinello and Rahman [3,4] developed their algorithm of variable MD cell shape to facilitate the prediction of solid–solid phase transitions. In classical NVE MD using cubic MD cell, the molecules must rearrange to achieve a phase transition from one

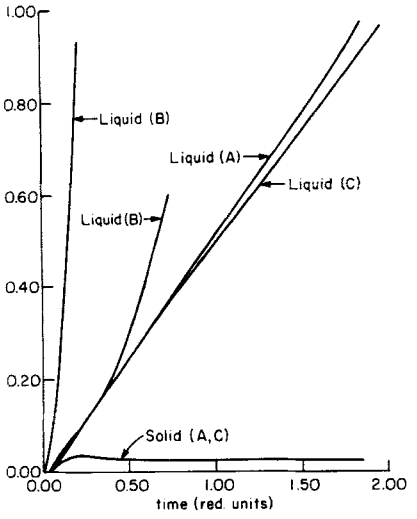

Figure 8 Mean square displacements are shown for the solid and the liquid state points of Table 1. A, B and C denote the three MD methods as in Figure 3.

crystal structure to another. Although the free energies of the two phases might favor such a transition, the process requires a large amount of computer time and is thus practially unfeasible. In the Parrinello-Rahman algorithm, the MD cell is allowed to change shape in response to the magnitude of the shear stress or the non-diagonal terms in the pressure tensor. Thus, the change from one lattice structure to another is achieved by changes in the shape of the MD cell rather than the direct rearrangement of the molecules. That such simulated transitions are feasible has been illustrated by various studies reported in the literature [4,6,8,9]. Recently, Ferrario and coworkers [37] studied the phase transition from the ordered monoclinic phase to a disordered tetragonal phase of t-butyl cyanide using the APR–NK algorithm. Although their results for the transition temperature did not compare well with the experimental value, such a transition is indeed observed experimentally.

In the present study, we have used the APR–NK algorithm to obtain the L^* at which transition from cubic Pa3 to orthorhomic CmCa and viceversa occurs in site-site diatomic systems with a large quadrupole moment ($Q^* = \sqrt{2}$). Simulations were carried out with 256 homonuclear diatomic molecules arranged in a MD cell with periodic boundary conditions. Runs were started either from cubic Pa3 or orthorhombic CmCa configurations. The Simulation conditions were fixed at $T^* = 0.25$ and $P^* = 0.10$.

In the first part of the study, the simulations were started from Pa3 configurations and with $L^* = 0.50$. About 1500 time steps were allowed for equilibration after which a run of 1500 time steps was made. L^* was then increased by 0.1 and using the configurations of the equilibrated system for $L^* = 0.50$, the process was repeated. This was continued for $L^* = 0.7$, 0.8, 0.9 and 0.95. Upto $L^* = 0.8$, only gradual changes in thermodynamic properties were observed, the MD cell fluctuating around the cubic shape, but at $L^* = 0.9$, the MD cell seemed to undergo a transition in shape and this was accompanied by a significant increase in density ρ^* from 0.575 to 0.593

Table 2 Phase Tranisition Properties for Cubic Pa3 to Orthorhombic CmCa Transition

		E^*		ρ^*				
Transition	L^*	Pa3	CmCa	Pa3	CmCa	ΔE^*	ΔH^*	ΔS^*
Pa3 to CmCa	0.90	−20.33	−20.92	0.575	0.593	−0.59	−0.595	−2.38
CmCa to Pa3	0.70	−21.78	−22.43	0.620	0.642	−0.65	−0.656	−2.62

and a decrease in internal energy E^* from −20.33 to −20.92. The resulting MD cell was found to fluctuate around an orthorhombic shape with sides in the ratio of approximately 1:1.1:1.25.

The process was next repeated in the reverse. Starting from orthorhombic configurations and $L^* = 0.90$, simulations were run at $L^* = 0.90$, 0.80, 0.70, and 0.60. A transition from orthorhombic to cubic was observed at $L^* = 0.70$. No significant changes in the shape of the MD cell were observed until the transition point, where in addition to the change in the shape of the MD cell, sharp changes in E^* were observed. The transition properties for the two transitions are summarized in Table 2.

The difference in the transition points for the two processes suggests that the MD simulations carried out with the time periods used here are successful in predicting spontaneous phase transitions, but the transition points are somewhat overpredicted. Thus by obtaining the phase transition from both the directions, the two bounds on the actual transition point are obtained. Such a behavior was suggested in an earlier study of melting transitions of diatomic solids at constant density [27]. For $0.7 < L^* < 0.9$ range we were unable to obtain any transition with the solid remaining in its starting structure either cubic or orthorhombic. The actual transition point, therefore, is in this range, but its accurate determination was not possible. It might be possible to reduce the uncertainty in the transition point by carrying out simulations for longer times. Q^* of $\sqrt{2}$ used here corresponds roughly to the quadrupole moment of 6.5×10^{-26} e.s.u. cm^2 for bromine [33]. For this value of Q, the results of English and Venables [36] indicate a transition from Pa3 to CmCa at $L^* = 0.80$, in agreement with our results.

To illustrate the structural difference between the cubic Pa3 and the orthorhombic CmCa lattices, we ran the simulation at $L^* = 0.85$ starting with cubic and then with orthorhombic configurations. We computed the angle average center–center and site–site correlation functions. These are shown in Figures 9 and 10. The two sets of functions show marked differences. A structural characteristic was also noted in the tilt angle of the molecules with respect to the lab fixed z-axis. Whereas in the cubic structure this angle fluctuated between 50° and 55°, in the orthorhombic case the molecules showed more tilt with fluctuations between 38° and 45°. This observation again is in agreement with the general results of English and Venables [36].

5. CONSTANT PRESSURE MELTING OF DIATOMIC SOLID

In a recent paper [27] we reported a MD simulation study of melting of a model site–site diatomic system ($L^* = 0.547$) with and without quadrupolar interactions ($Q^* = 0$ and $Q^* = 1.0$) at constant density $\rho^* = 0.625$. The effect of quadrupole moment on the thermodynamic and structural properties of the liquid and the solid

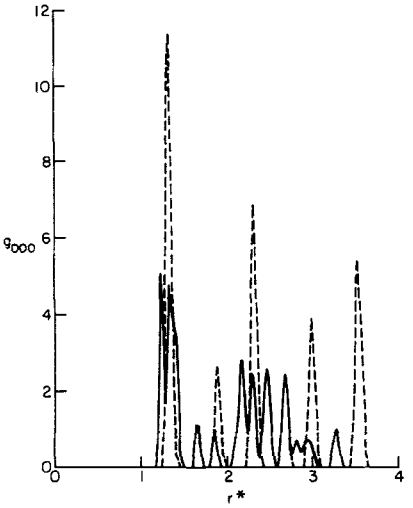

Figure 9 Center–Center average correlation functions are shown for the cubic Pa3 and orthorhombic CmCa solids of diatomic molecules ($L^* = 0.85$, $Q^* = \sqrt{2}$) at low temperature and pressure ($T^* = 0.25$, $P^* = 0.10$).

close to the melting temperature was investigated. It was found that the addition of the quadrupolar interactions increased the melting temperature and the entropy of melting considerably. The reason for this was that the imposition of the quadrupole moment induced structural changes such that the configurational internal energy of the solid was reduced more than that of the corresponding liquid at the melting point. The increased stability of the solid led to higher melting point and higher entropy of melting.

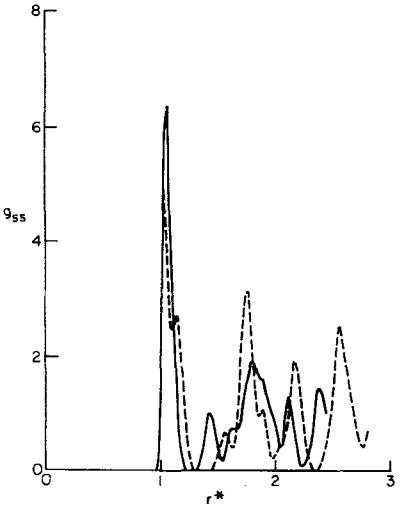

Figure 10 For the same diatomic systems as in Figure 9, site–site correlation functions are shown.

However, most melting processes occur at constant pressure. We, therefore, carried out an isobaric melting study of the same diatomic model systems using the APR–NK and the EEM MD simulations. Isothermal algorithm of Evans and coworkers [2,13,14] was used in the EEM algorithm, whereas no efforts were made to hold temperature constant in the APR–NK algorithm. The purpose of the work was to identify the transition temperatures and to study the effect of the quadrupole moment and the pressure on the thermodynamic and structural properties at melting transition. A number of simulations were carried out to obtain the melting transitions for the following systems: (1) $Q^* = 0$, $P^* = 0.10$; (2) $Q^* = 1.0$, $P^* = 0.10$; (3) $Q^* = 1.0$, $P^* = 2.25$; (4) $Q^* = 1.0$, $P^* = 5.0$ and (5) $Q^* = 1.0$, $P^* = 10.0$. Some of the simulations used the APR–NK algorithm and others the EEM algorithm. All the simulations were carried out by starting from a very low temperature fcc α-N_2 structure and slowly increasing the temperature during the equilibration stage until the desired temperature was reached. As in the constant density study [27] we were unable to obtain freezing of a liquid because nucleation of a liquid to proper crystal lattice would take a much longer time than is feasible in these computer simulations.

A summary of the simulations and the thermodynamic properties is given in Table 3. In Figures 11–13 we have plotted E^* and ρ^* v/s T^* through the transition point for the five studies. The estimated transition temperatures are marked by vertical lines. It is difficult to compare these results with the corresponding results at constant density. However, by careful analysis of these data and those of [27], we observed that at constant pressure solids tend to melt at slightly lower temperatures (by less than 0.05 reduced units) than at constant density. Even so, the estimated transition temperatures T^*_m give the upper bounds for the actual melting points of the solids. In the absence of a method to calculate chemical potentials for these systems it is

Table 3 Thermodynamic Properties from Constant Pressure MD Simulation runs to predict melting transitions.

Type of Algorithm	N_t	$t^* \times 10^4$	T^*	P^*	ρ^*	E^*
$L^* = 0.547$, $Q^* = 0$						
EEM	5000	5	0.75	0.10	0.6436	−17.71
EEM	5000	5	0.80	0.10	0.6091	−16.36
EEM	5000	5	1.00	0.10	0.5884	−15.57
$L^* = 0.547$, $Q^* = 1.0$						
APR–NK ($M = 5$)	5000	10	1.00	0.10	0.6616	−20.48
APR–NK ($M = 2$)	5000	5	1.306	0.10	0.6326	−19.00
EEM	5000	5	1.34	0.17	0.6293	−18.78
APR–NK ($M = 5$)	6500	5	1.391	0.10	0.5462	−14.55
APR–NK ($M = 0.2$)	6000	5	1.527	0.10	0.5318	−14.01
EEM	5000	5	1.43	2.30	0.6434	−18.94
EEM	5000	5	1.48	2.21	0.5756	−15.10
EEM	5000	5	1.55	2.21	0.5664	−14.74
APR–NK ($M = 1$)	5000	5	1.395	5.0	0.6715	−19.76
EEM	5000	5	1.50	5.04	0.6632	−19.28
APR–NK ($M = 1$)	7500	3	1.564	5.0	0.6114	−15.91
APR–NK ($M = 0.5$)	5000	3	1.669	5.0	0.6003	−15.39
APR–NK ($M = 1$)	5000	5	1.526	10.0	0.6943	−19.76
EEM	5000	5	1.65	10.13	0.6875	−19.31
APR–NK ($M = 1$)	9000	3	1.70	10.0	0.6452	−16.31
APR–NK ($M = 1$)	7500	3	1.851	10.0	0.6297	−15.38

Table 4 Isobaric melting data for diatomics ($L^* = 0.547$)

	$Q^* = 0$	$Q^* = 1.0$			
	$P^* = 0.10$	$P^* = 0.10$	$P^* = 2.25$	$P^* = 5.0$	$P^* = 10.0$
T^*_m	0.78 ± 0.02	1.37 ± 0.02	1.46 ± 0.02	1.53 ± 0.02	1.68 ± 0.01
ΔE^*_m	1.13 ± 0.04	4.01 ± 0.06	3.62 ± 0.06	3.06 ± 0.06	2.73 ± 0.06
ΔH^*_m	1.21 ± 0.05	4.24 ± 0.07	3.79 ± 0.07	3.17 ± 0.07	2.82 ± 0.07
ΔS^*_m	1.58 ± 0.06	3.11 ± 0.07	2.60 ± 0.08	2.07 ± 0.08	1.68 ± 0.08

difficult to determine the melting temperature exactly. The melting data for the different systems are reported in Table 4. A comparison of the melting data for $Q^* = 0$, $P^* = 0.10$ and $Q^* = 1.0$, $P^* = 0.10$ gives the effect of quadrupolar interaction on melting. Analogous to the constant density transition [27], the quadrupole moment has considerable effect on the melting properties as reflected by the large increases in the T^*_m and the entropy of melting ΔS^*_m. The reason for this is that the quadrupolar interaction decreases the internal energy of the solid at the melting point considerably as observed by comparing the internal energies of the two solids corresponding to $Q^* = 0$ and $Q^* = 1.0$ at the melting points. The solid with $Q^* = 0$ has $E^* = -18.7$ which is much lower than $E^* = -17.5$ for the solid with $Q^* = 0$, in spite of the fact that the latter solid is at a appreciably lower temperature. In contrast, Q^* does not contribute much to the liquid E^* at the melting point. ($E^* = -16.4$ at $Q^* = 0$ and $E^* = -14.7$ at $Q^* = 1.0$. The higher E at $Q^* = 1.0$ is due to the higher temperature of that liquid.) The combined effect, therefore, leads to considerably higher ΔE^*_m at $Q^* = 1.0$.

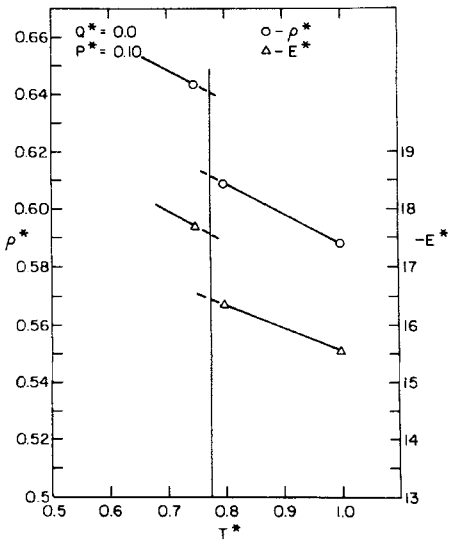

Figure 11 Simulated values of the reduced density ρ^* and average configurational energy E^* are plotted vs. reduced temperature T^* for the system $Q^* = 0$, $P^* = 0.10$. The estimated melting temperature T^*_m is indicated by the vertical line at $T^* = 0.78$, and the dashed lines are linear extrapolations of the data into the melting region.

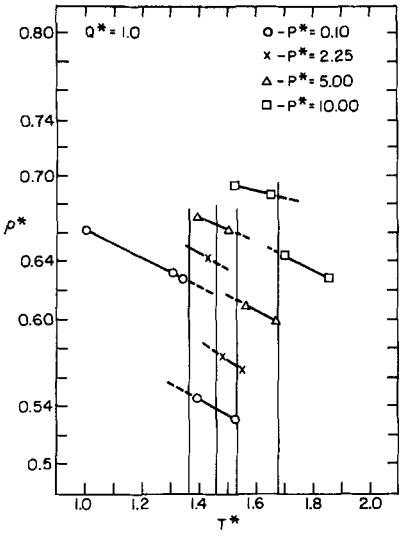

Figure 12 Simulated values for the reduced density ρ^* are plotted vs T^* for the four systems with $Q^* = 1.0$. Again melting temperatures are indicated by vertical lines.

This is further illustrated by the structural properties of the solids and the liquids for the two cases. In Figures 14–17 we have plotted the site–site correlation functions g_{ss} and some coefficients (g_{000}, g_{200}, and g_{220}) of the spherical harmonic expansion of the center of mass pcf. Each figure shows the functions for the solid and the corresponding liquid closest to the melting point. The contribution to the internal energy from the quadrupolar interaction can be written as a sum of integrals involving only

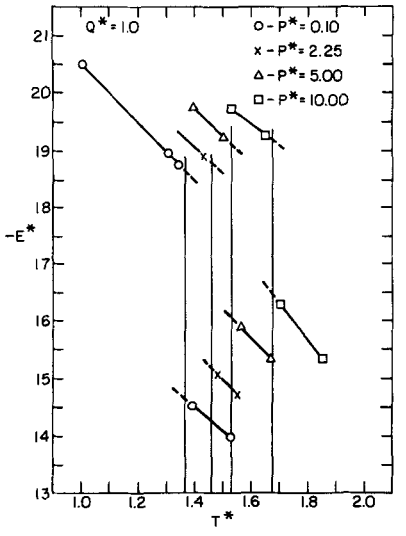

Figure 13 Same as Figure 12 but E^* are plotted vs T^*.

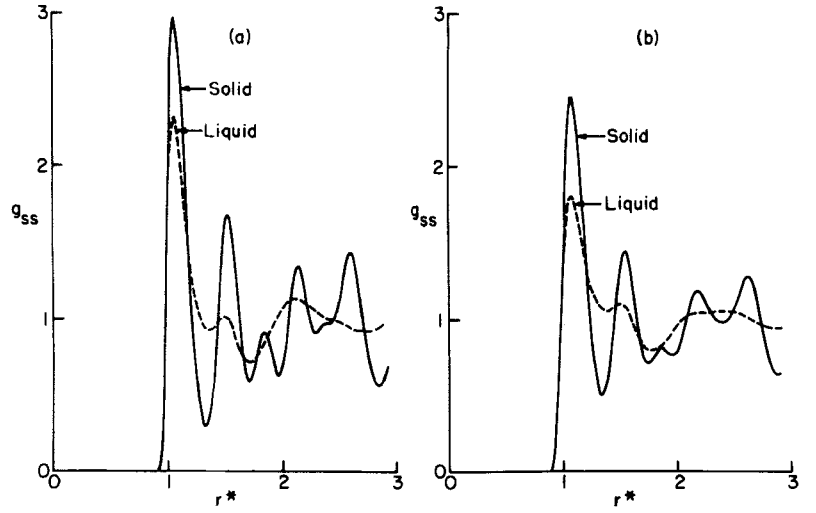

Figure 14 Site-site correlation functions for the solid and the liquid close to the transition are plotted as a function of reduced separation distance r^* for the two cases: (a) $Q^* = 0$, $P^* = 0.1$, (b) $Q^* = 1.0$, $P^* = 0.1$.

the coefficients g_{220}, g_{221}, and g_{222}. The large effect of Q^* on E^* of the solids is explained from the large initial negative peaks in g_{220} and g_{221}. The effect of quadrupole moment is to increase the magnitude of these peaks, leading to a substantial increase in $-E^*$. Such features are absent in the case of the liquids. Qualitatively, the structural properties for the isobaric transitions are in no way different than the corresponding ones at constant density. A more detailed analysis and discussion of the structures of such solids and liquids is given in [27].

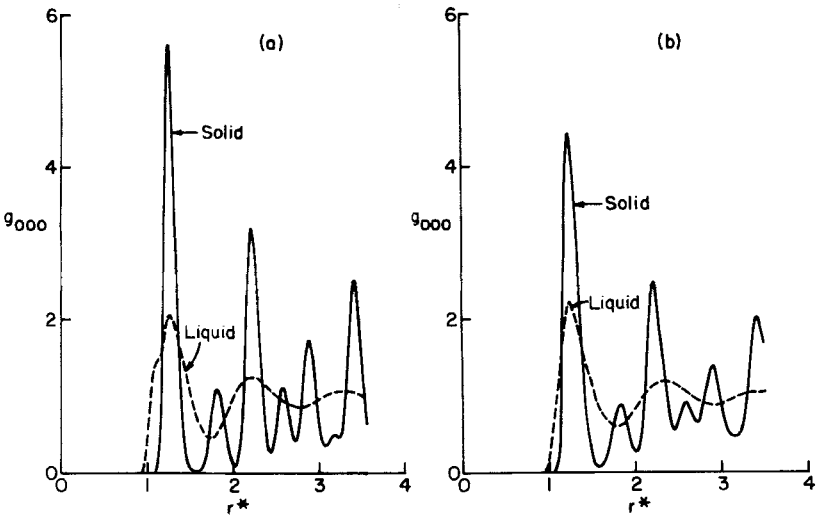

Figure 15 Same as Figure 14 but g_{000} is plotted.

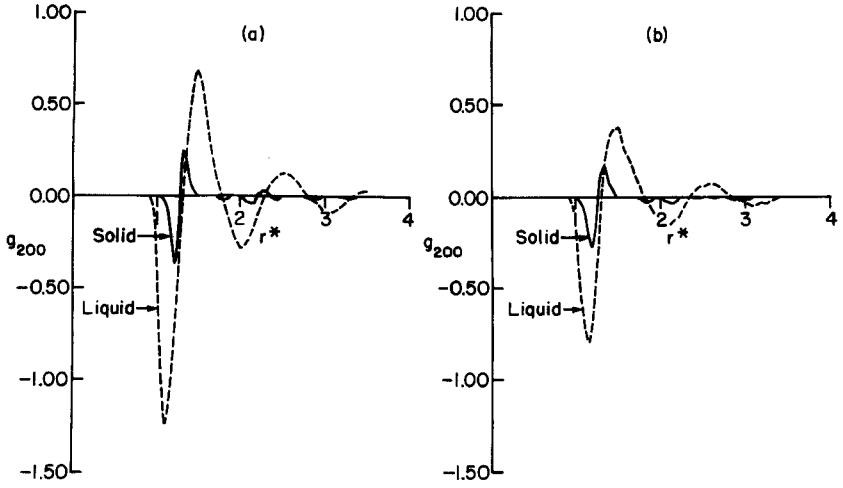

Figure 16 Same as Figure 14 but shows g_{200}

With increased pressure, the melting temperature T^*_m increases; on the other hand the entropy of melting ΔS^*_m and $\Delta\rho^*$ decrease, consistent with the usual experimental observations. At higher pressures no qualitative differences in structural properties were observed.

CONCLUSIONS

We derive the following conclusions from this work:

1. The isobaric algorithms of Andersen, and Evans and Morriss when applied to

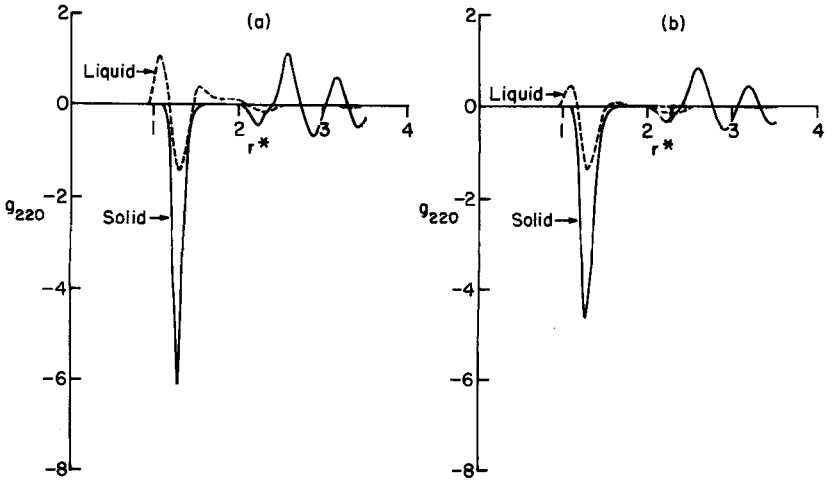

Figure 17 Same as Figure 14 but shows g_{220}

diatomic liquids and solids give equivalent thermodynamic and structural information. The two algorithms, however, exhibit different magnitudes of fluctuations for different quantities, and as a result are not equivalent when computing properties from fluctuations. Specifically, Evans and Morriss algorithm is better for calculating isobaric heat capacities, because the pressure in this method is held identically constant.

2. Rotational dynamics of molecules observed in the EEM simulations agree well with equivalent results in the microcanonical ensemble. However, differences are observed with respect to translational dynamics. In the EEM simulations, differences are observed in the velocity correlation functions calculated from the generalized momenta and those calculated from the linear velocities of the molecules. The diffusion coefficients calculated from these two functions vary by as much as 5%. Although the former show better agreement with the Newtonian translational dynamics, the diffusion coefficient is rigorously defined in terms of the latter function.

3. The use of the Parrinello-Rahman algorithm to simulate solid-solid phase transition in diatomic systems is once more illustrated. Spontaneous transition from cubic Pa3 to orthorhombic CmCa and viceversa has been successfully simulated. Although the transition point could not be determined precisely, the results show qualitative agreement with previous studies [36] and experimental observations.

4. Isobaric melting studies have been carried out for model diatomic solids with and without quadrupolar interactions. The quadrupole moment results in stabilizing the solid, and hence increases the melting point considerably. This observation is in agreement with the conclusion of a previous study on melting of similar systems at constant density [27]. The simulated pressure effect on melting in these systems is in agreement with general experimental observations.

APPENDIX

Constant Pressure and Constant Temperature Constraints in EEM Algorithm

The constant pressure constraint is given by Equation (14). The second term on the right hand side of Equation (14) is divided into two parts, one for $q_{ij} < q_c$, and the other is the cut-off correction for $q_{ij} > q_c$, where q_c is the cut-off distance. The first term on r.h.s. of Equation (14) disappears because of the constant temperature constraint (Equation 16)). The other two terms require the evaluation of $\dot{F}_{ij}$ for the site–site L-J and the ideal point quadrupolar potentials.

$\tilde{\dot{F}}_{ij}$ for the site-site LJ potential

Force $\tilde{F}_{ij}$ is the summation of the forces between individual atoms m on molecule i and n on molecule j, hence,

$$\tilde{\dot{F}}_{ij} = \sum_{m=1}^{2} \sum_{n=1}^{2} \tilde{\dot{F}}_{mn} \tag{A.1}$$

If $\tilde{q}_{mn}$ is the vector joining the centers of atoms m and n and u is the potential between atoms m and n, then it may be shown that

$$\dot{\tilde{F}}_{mn} = A\,\dot{\tilde{q}}_{mn} + B\,(\tilde{q}_{mn} \cdot \dot{\tilde{q}}_{mn})\,\tilde{q}_{mn} \tag{A.2}$$

where

$$A = -\frac{1}{|q_{mn}|}\frac{du}{dq_{mn}} \tag{A.3}$$

$$B = \frac{1}{|q_{mn}|}\frac{dA}{dq_{mn}} \tag{A.4}$$

$\tilde{q}_{mn}$ may be written in terms of $\tilde{q}_{ij}$ as

$$\tilde{q}_{mn} = \tilde{q}_{ij} + \tilde{H}_{mn} \tag{A.5}$$

where

$$\tilde{H}_{mn} = \tilde{H}_m - \tilde{H}_n \tag{A.6}$$

$\tilde{H}_m$ is the vector from the center of molecule i to the atom m and $\tilde{H}_n$ is the vector from the center of molecule j to the atom n. Substituting Equations (8) and (A.5) into Equation (A.2) we get

$$\dot{\tilde{F}}_{mn} = A\left(\frac{\tilde{p}_{ij}}{m} + \dot{\varepsilon}\,\tilde{q}_{ij} + \dot{\tilde{H}}_{mn}\right) + B\left[(\tilde{q}_{ij} + \tilde{H}_{mn}) \cdot \left(\frac{\tilde{p}_{ij}}{m} + \dot{\varepsilon}\,\tilde{q}_{ij} + \dot{\tilde{H}}_{mn}\right)\right](\tilde{q}_{ij} + \tilde{H}_{mn}) \tag{A.7}$$

$\dot{\tilde{F}}_{ij}$ for the site–site LJ potential may be obtained by substituting Equation (A.7) into Equation (A.1)

$\dot{\tilde{F}}_{ij}$ for ideal point quadrupolar potential

Ideal point quadrupolar potential between molecules i and j is given by Equation (37). For such analytical potentials between axially symmetric molecules, force between the molecules is given by [23]

$$\tilde{F}_{ij} = -\left[\tilde{q}_{ij}\left(\frac{1}{|q_{ij}|}\frac{\partial u_{ij}}{\partial q_{ij}}\right) + \left(\hat{H}_i - \frac{\tilde{q}_{ij}}{|q_{ij}|}C_i\right)\frac{1}{|q_{ij}|}\frac{\partial u_{ij}}{\partial C_i} + \left(\hat{H}_j - \frac{\tilde{q}_{ij}}{|q_{ij}|}C_j\right)\frac{1}{|q_{ij}|}\frac{\partial u_{ij}}{\partial c_{ij}}\right] \tag{A.8}$$

where

$$C_i = \hat{H}_i \cdot \hat{q}_{ij}$$

$$C_j = \hat{H}_j \cdot \hat{q}_{ij}$$

and

$$C_{ij} = \hat{H}_i \cdot \hat{H}_j$$

$\hat{H}_i$ and $\hat{H}_j$ are unit vectors along the axes of molecules i and j and $\hat{q}_{ij}$ is a unit vector along the line joining the centers of molecules i and j we write $\tilde{F}_{ij}$ as

$$\tilde{F}_{ij} = -\left[\tilde{V}_1 D_1 + \tilde{V}_2 D_2 + \tilde{V}_3 D_3\right] \tag{A.9}$$

where

$$\tilde{V}_1 = \tilde{q}_{ij},\ \tilde{V}_2 = \left(\hat{H}_i - \frac{\tilde{q}_{ij}}{|q_{ij}|} C_i\right), \text{ and } \tilde{V}_3 = \left(\hat{H}_j - \frac{\tilde{q}_{ij}}{|q_{ij}|} C_j\right) \tag{A.10}$$

$$D_1 = \frac{1}{|q_{ij}|}\frac{\partial u_{ij}}{\partial q_{ij}},\ D_2 = \frac{1}{|q_{ij}|}\frac{\partial u_{ij}}{\partial C_i}, \text{ and } D_3 = \frac{1}{|q_{ij}|}\frac{\partial u_{ij}}{\partial C_j} \tag{A.11}$$

$\dot{\tilde{F}}_{ij}$ is then given as

$$\dot{\tilde{F}}_{ij} = -\sum_{i=1}^{3} (\tilde{V}_i \dot{D}_i + \dot{\tilde{V}}_i D_i) \tag{A.12}$$

Expressions for $\dot{\tilde{V}}_i$ and $\dot{\tilde{D}}_i$ may be easily obtained, and substituting for $\dot{\tilde{q}}_{ij}$ in these expressions from Equation (8), the final equation for $\dot{\tilde{F}}_{ij}$ may be obtained.

Correction terms

The correction terms are the terms for $q_{ij} > q_c$ in Equation (14). These are evaluated assuming the pcf to be unity for $q_{ij} > q_c$. There is no contribution from the quadrupolar potential as both $\tilde{F}_{ij}$ and $\dot{\tilde{F}}_{ij}$ integrated over all the relative orientations of molecules i and j give zeroes. The correction term because of diatomic potential is written as

$$\begin{aligned}
&\sum_{i=1}^{N}\sum_{j<i} (\dot{\tilde{q}}_{ij} \cdot \tilde{F}_{ij} + \tilde{q}_{ij} \cdot \dot{\tilde{F}}_{ij})_{q_{ij} > q_c} \\
&\quad = \sum_{i=1}^{N}\sum_{j<i}\left[\left(\frac{\tilde{p}_{ij}}{m} + \dot{\varepsilon}\,\tilde{q}_{ij}\right) \cdot \tilde{F}_{ij} + q_{ij} \cdot \dot{\tilde{F}}_{ij}\right]_{q_{ij} > q_c} \\
&\quad = \sum_{i=1}^{N}\sum_{j<i}\sum_{m=1}^{2}\sum_{n=1}^{2} [\dot{\varepsilon} A(\tilde{q}_{ij} \cdot \tilde{q}_{mn}) + \dot{\varepsilon}\{A|q_{ij}|^2 + B|q_{ij}|^4\}]_{q_{ij} > q_c}
\end{aligned} \tag{A.13}$$

Replacing the summations by integration we obtain

$$8\pi\rho N \int_{q_c}^{\infty} \dot{\varepsilon}\,[2Aq^2 + Bq^4]\, q^2\, dq = 384\pi\rho N\dot{\varepsilon}\,[q_c^{-3} - \frac{4}{3} q_c^{-9}] \tag{A.14}$$

Overall equation for $\dot{\varepsilon}$

Substituting $\dot{F}_{ij}$ for diatomic potentials and the correction term in equation (14), the overall equation for $\dot{\varepsilon}$ is obtained and is given below.

$$\dot{\varepsilon}\left[9PV + 384\pi\rho N\left(\frac{4}{3} q_c^{-9} - q_c^{-3}\right) - \sum_{i=1}^{N}\sum_{j<i}\sum_{m=1}^{2}\sum_{n=1}^{2} B\,(\tilde{q}_{mn} \cdot \tilde{q}_{ij})^2\right.$$

$$
\begin{aligned}
&- \left\{ \sum_{i=1}^{N} \sum_{j<i} (\tilde{q}_{ij} \cdot \tilde{F}_{ij}) + (\text{A-D}_1)\, |q_{ij}|^2 - (|q_{ij}|^3) \frac{\partial D_1}{\partial q_{ij}} \right\} \Bigg] \\
&= \sum_{i=1}^{N} \sum_{j<i} \sum_{m=1}^{2} \sum_{n=1}^{2} A\, (\tilde{q}_{ij} \cdot \dot{\tilde{H}}_{mn}) \\
&+ \sum_{i=1}^{N} \sum_{j<i} \sum_{m=1}^{2} \sum_{n=1}^{2} B \left\{ \left(\tilde{q}_{mn} \cdot \frac{\tilde{p}_{ij}}{m} \right) + (\tilde{q}_{mn} \cdot \dot{\tilde{H}}_{mn}) \right\} (\tilde{q}_{ij} \cdot \tilde{q}_{mn}) \\
&+ \sum_{i=1}^{N} \sum_{j<i} \frac{\tilde{p}_{ij}}{m} \cdot \tilde{F}_{ij} + (\text{A-D}_1) \frac{\tilde{q}_{ij} \cdot \tilde{p}_{ij}}{m} + D_2 \left(\tilde{V}_2 \cdot \frac{\tilde{p}_{ij}}{m} \right) \\
&+ D_3 \left(\tilde{V}_3 \cdot \frac{\tilde{p}_{ij}}{m} \right) - |q_{ij}|^2 \left[\frac{\partial D_1}{\partial q_{ij}} \frac{\tilde{q}_{ij} \cdot \tilde{p}_{ij}}{m|q_{ij}|} + \frac{\partial D_1}{\partial C_i} \left\{ \dot{\hat{H}}_i \cdot \frac{\tilde{q}_{ij}}{|q_{ij}|} \right. \right. \\
&+ \left. \frac{1}{|q_{ij}|} \left(\tilde{V}_2 \cdot \frac{\tilde{p}_{ij}}{m} \right) \right\} + \frac{\partial D_1}{\partial C_j} \left\{ \dot{\hat{H}}_j \cdot \frac{\tilde{q}_{ij}}{|q_{ij}|} + \frac{1}{|q_{ij}|} \left(\tilde{V}_3 \cdot \frac{\tilde{p}_{ij}}{m} \right) \right\} \\
&+ \left. \frac{\partial D_1}{\partial C_{ij}} (\dot{\hat{H}}_i \cdot \hat{H}_j + \hat{H}_i \cdot \dot{\hat{H}}_j) \right]
\end{aligned}
\tag{A.15}
$$

The equations for α and α_1 are

$$
\alpha = \frac{\sum_{i=1}^{N} \tilde{p}_i \cdot \tilde{F}_i}{\sum_{i=1}^{N} p_i^2} - \dot{\varepsilon} \tag{A.16}
$$

$$
\alpha_1 = \frac{\frac{1}{I} \sum_{i=1}^{N} \tilde{\omega}_{pi} \cdot \tilde{N}_{pi}}{\sum_{i=1}^{N} \omega_{pi}^2} \tag{A.17}
$$

where $I = I_{px} = I_{py}$

References

[1] H.C. Andersen, "Molecular Dynamics Simulations at Constant Pressure and/or Temperature", *J. Chem. Phys.*, **72**, 2384 (1980).

[2] D.J. Evans and G.P. Morriss, "Isothermal-Isobaric Molecular Dynamics", *Chem. Phys.*, **77**, 63 (1983).

[3] M. Parrinello and A. Rahman, "Crystal Structure and Pair Potentials: A Molecular Dynamics Study", *Phys. Rev. Lett.*, **45**, 1196 (1980).

[4] M. Parrinello and A. Rahman, "Polymorphic Transitions in Single Crystals: A New Molecular Dynamics Method", *J. Appl. Phys.*, **52**, 7182 (1981).

[5] H.J.C. Berendsen, J.P.M. Postma, W.F. Van Gunsteren, A. DiNola and J.R. Haak, "Molecular Dynamics with Coupling to an External Bath", *J. Chem. Phys.*, **81**, 3684 (1984).

[6] G.S. Pawley and G.W. Thomas, "Computer Simulation of the Plastic-to-Crystalline Phase Transition in SF_6 ", *Phys. Rev. Lett.*, **48**, 410 (1982).

[7] S. Nosé and M.L. Klein, "Constant Pressure Molecular Dynamics for Molecular Systems", *Molec. Phys.*, **50**, 1055 (1983).
[8] S. Nosé and M.L. Klein, "Structural Transformations in Solid Nitrogen at High Pressure", *Phys. Rev. Lett.*, **50**, 1207 (1983).
[9] S. Nosé and M.L. Klein, "A Study of Solid and Liquid Carbon Tetrafluoride Using the Constant Pressure Molecular Dynamics Technique", *J. Chem. Phys.*, **78**, 6928 (1983).
[10] J.P. Ryckaert and G. Ciccotti, "Introduction of Anderson's Demon in the Molecular Dynamics of Systems with Constraints", *J. Chem. Phys.*, **78**, 7368 (1983).
[11] M. Ferrario and J.P. Ryckaert, "Constant Pressure-Constant Temperature Molecular Dynamics for Rigid and Partially Rigid Molecular Systems", *Molec. Phys.* **54**, 587 (1985).
[12] J.E. Coon, S. Gupta and E. McLaughlin, "Isothermal-Isobaric Molecular Dynamics Simulation of Diatomic liquids and Their Mixtures", *Chem. Phys.*, **113**, 43 (1987).
[13] W.G. Hoover, A.J.C. Ladd and B. Moran, "High-Strain-Rate Plasic Flow Studied Via Non-equilibrium Molecular Dynamics", *Phys. Rev. Lett.*, **48**, 1818 (1982).
[14] D.J. Evans, "Computer Experiment for Nonlinear Thermodynamics of Couette Flow", *J. Chem. Phys.*, **78**, 3297 (1983).
[15] S. Nosé, "A Molecular Dynamics Method for Simulations in the Canonical Ensemble", *Molec. Phys.*, **52**, 255 (1984).
[16] S. Nosé "A Unified Formulation of the Constant Temperature Molecular Dynamics Methods", *J. Chem. Phys.*, **81**, 511 (1984).
[17] D.J. Evans and B.L. Holian, "The Nosé - Hoover Thermostat", *J. Chem. Phys.*, **83**, 4069 (1985).
[18] J.M. Haile and S. Gupta, "Extensions of the Molecular Dynamics Simulation Method. II. Isothermal Systems", *J. Chem. Phys.*, **79**, 3067 (1983).
[19] J. Jellinek, "Dynamics for Nonconservative Systems: Ergodicity Beyond the Microcanonical Ensemble", *J. Phys. Chem.*, **92**, 3163 (1988).
[20] W.G. Hoover, D.J. Evans, R.B. Hickman, A.J.C. Ladd, W.T. Ashurst and B. Moran, "Lennard-Jones Triple-Point Bulk and Shear Viscosities, Green-Kubo Theory, Hamiltonian Mechanics, and Nonequilibrium Molecular Dynamics", *Phys. Rev. A.*, **22**, 1690 (1980).
[21] R. Edberg, D.J. Evans and G.P. Morriss, "Constrained Molecular Dynamics: Simulations of Liquid Alkanes with a New Algorithm", *J. Chem. Phys.*, **84**, 6933 (1986).
[22] H. Goldstein, "Classical Mechanics", Addison-Wesley Publishing Company, Inc. (1980).
[23] P.S.Y. Cheung, "On the Efficient Evaluation of Torques and Forces for Anisotropic Potentials in Computer Simulation of Liquids Composed of Linear Molecules", *Chem. Phys. lett.*, **40**, 19 (1976).
[24] D.J. Evans and G.P. Morriss, "The Isothermal/Isobaric Molecular Dynamics Ensemble", *Phys. Lett.*, **98a**, 433 (1983).
[25] D.J. Evans and G.P. Morriss, "Non-Newtonian Molecular Dynamics" *Comp. Phys. Rep.*, **1**, 297 (1984).
[26] D. Brown and J.H.R. Clarke, "A Comparison of Constant Energy, Constant Temperature and Constant Pressure Ensembles in Molecular Dynamics Simulations of Atomic Liquids", *Molec. Phys.*, **51**, 1243 (1984).
[27] V. Kabadi and W.A. Steele, "Simulation Study of Melting for Diatomic Molecules with Quadrupolar Interactions", *J. Phys. Chem.*, **89**, 743 (1985).
[28] J.L. Lebowitz, J.K. Percus and L. Verlet, "Ensemble Dependence of Fluctuations with Application to Machine Computations", *Phys. Rev.*, **153**, 250 (1967).
[29] P.S.Y. Cheung, "On the Calculation of Specific Heats, Thermal Pressure Coefficients and Compressibilities in Molecular Dynamics Simulations", *Molec. Phys.*, **33**, 519 (1977).
[30] J.M. Haile and H.W. Graben, "On the Isoenthalpic-Isobaric Ensemble in Classical Statistical Mechanics", *Molec. Phys.*, **40**, 1433 (1980).
[31] J.R. Ray, H.W. Graben, and J.M. Haile, "Statistical Mechanics of the Isoenthalpic-Isobaric Ensemble", *Il Nuovo Cimento*, **64**, 191 (1981).
[32] W.A. Steele, "Statistical Mechanics of Nonspherical Molecules", *J. Chem. Phys.*, **39**, 3197 (1963).
[33] W.B. Streett and D.J. Tildesley, "Computer Simulations of Polyatomic Molecules II. Molecular Dynamics Studies of Diatomic Liquids with Atom-Atom and Quadrupole-Quadrupole Potentials", *Proc. R. Soc. (Lond) A.* **355**, 239 (1977).
[34] D.J. Evans and G.P. Morriss, "Equilibrium Time Correlation Functions Under Gaussian Isothermal Dynamics", *Chem. Phys.*, **87**, 451 (1984).
[35] See for example J.P. Hansen and I.R. McDonald, "Theory of Simple Liquids", 2nd edition, Chap. 7., Academic Press, London (1986).
[36] C.A. English and J.A. Venables, "The Structure of the Diatomic Molecular Solids", *Proc. R. Soc. (Lond) A.* **340**, 57 (1974).
[37] M. Ferrario, M.L. Klein and I.R. McDonald, "Structure of Solid t-Butyl Cyanide: A Study by Means of Constant-Temperature, Constant-Pressure, Molecular Dynamics Simulations", *J. Chem. Phys.*, **87**, 4823 (1987).